

The QCD Phase Diagram from Statistical Model Analysis

Francesco Becattini

Universita di Firenze and INFN Sezione di Firenze, Firenze

Marcus Bleicher, Jan Steinheimer

Frankfurt Institute of Advanced Studies (FIAS), Frankfurt

Reinhard Stock

Frankfurt Institute of Advanced Studies (FIAS), Frankfurt

Institut fuer Kernphysik, Goethe Universitaet, Frankfurt

Ideally, the Statistical Hadronization Model (SHM) freeze-out curve should reveal the QCD parton-hadron phase transformation line in the (T, μ_B) plane. We discuss the effects of various final state interaction phenomena, like baryon-antibaryon annihilation, core-corona effects or QCD critical point formation, which shift or deform the SHM freezeout curve. In particular, we present a method to remove the annihilation effects by quantifying them with the microscopic hadron transport model UrQMD. We further discuss the new aspects of hadronization that could be associated with the relatively broad cross-over phase transformation as predicted by lattice-QCD theory at low μ_B . That opens up the possibility that various observables of hadronization, e.g. hadron formation or susceptibilities of higher order (related to grand canonical fluctuations of conserved hadronic charges) may freeze out at different characteristic temperatures. This puts into question the concept of a universal (*pseudo-critical*) temperature, as does the very nature of a cross-over phase transformation.

1. Introduction

The phase diagram of strongly interacting matter, as addressed by the thermodynamics of Quantum Chromodynamics (QCD) theory, represents one of the open problems of the Standard Model of elementary interactions. Thermal QCD confronts matter at high energy density, as was prevailing during the early phases of the cosmological expansion but can also be investigated (albeit not at macroscopic scale) in collisions of heavy nuclei at relativistic energy. One thus creates a hot and compressed *fireball* in which, for an instant of time, the QCD confinement of partons into hadrons is overcome, creating a hot partonic QCD plasma state, the so-called

2 *Reinhard Stock*

Quark-Gluon Plasma(QGP). It is the goal, both of experiment and of QCD thermodynamics, to elaborate the phase diagram of *fireball matter*. Its most prominent feature, the transition line between hadrons and partons, in the plane spanned by temperature T and baryochemical potential μ_B , is located in the nonperturbative sector of QCD. Here, the theory can (only) be solved on the lattice,¹ within the above variables T and μ_B , and has recently led to predictions of the parton-hadron boundary line.^{2,3}

This line can also be addressed by experiment, in relativistic collisions of heavy nuclei where the primordial interaction volume is far from equilibrium at first; but after a small relaxation time (of order 1 fm/c, or even less) it settles onto the equilibrium (T, μ_B) plane at a temperature well above the *critical* (or pseudocritical) temperature T_c that corresponds to the phase transformation. Expansion and cooling then take the fireball down to the QCD phase boundary where hadronization occurs(4), with the parameters $(T_c, \mu_{B,c})$ being preserved in the relative abundances (multiplicities) of the various created hadronic species.^{4,5} Assuming, for the moment, that these multiplicities are conserved throughout the final hadron-resonance cascade expansion, their analysis in the framework of the Statistical Hadronization Model(SHM)⁴⁻⁸ reveals the hadronization point, at which, in this ideal picture, the partons freeze-out into hadrons.⁹⁻¹¹ The hadron abundances stay essentially unobliterated throughout the ensuing hadron/resonance expansion evolution. The latter fixes flow observables, spectra and Bose correlations. So there are two separate, well spaced freeze-outs, the so-called hadro-chemical and the kinetic ones.

As the primordial temperature (baryochemical potential) shifts upward (downward) with increasing collision energy, an ascending sequence of experimental energies can, thus, map a sequence of hadronization points along the QCD parton-hadron boundary line. At the low AGS energies, in the domain of $\sqrt{s} = 5$ GeV, this investigation begins at μ_B of about 550 MeV, falling to about 250 MeV at top SPS energy ($\sqrt{s} = 17.3$ GeV), then on to the 20 to 100 MeV domain at RHIC energies (\sqrt{s} from 60 to 200 GeV), and ending at baryochemical potential practically zero at the LHC energy of 2.76 TeV, in central collisions of Pb or Au projectiles.^{6,7,12} It is here that we meet with the conditions prevailing in the big-bang expansion, thus recreating the cosmological phase transition to hadrons that occurred at a few microseconds time.

With these assumptions which of course need careful discussion and refinement, the subject of the present article, one of the main goals common to QCD theory and nuclear collision experiments — the parton-hadron boundary line — comes well within reach as we shall demonstrate in the following. We will describe the state of the art in applying the SHM to the hadron multiplicity results created at the AGS, SPS, RHIC and LHC (also discussing difficulties arising in the application of the statistical model), and compare the resulting hadronization curve with the corresponding lattice QCD calculations.

Turning to a more detailed argumentation, we note that at present the identifi-

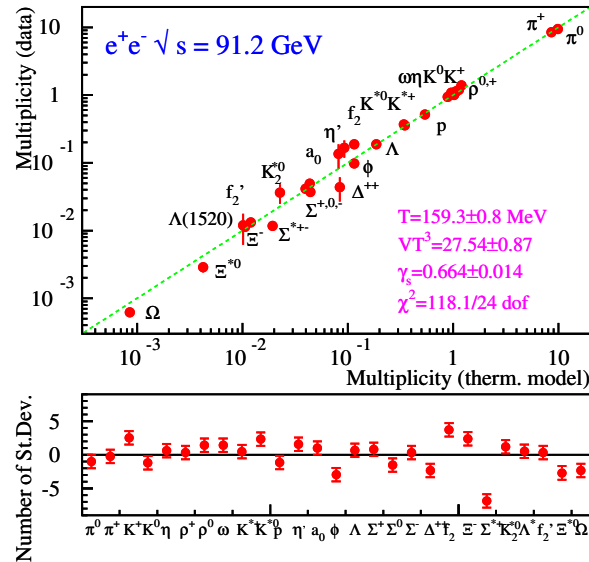


Fig. 1. Hadron production in electron-positron annihilation at LEP energy, confronted with canonical Statistical Hadronization Model calculations.¹⁵

cation of the QCD hadronization point with the emergence of a hadron/resonance population that is “born into equilibrium”,⁹ thus resembling an equilibrium canonical or grand-canonical Gibbs ensemble (the basis of the Statistical Hadronization Model^{4,5}), remains a (plausible) conjecture. No analytic solution of the QCD Lagrangian exists in the non-perturbative domain. Two approaches nevertheless suggest the validity of this assumption. The first is a line of argument developed by Amati, Veneziano and Webber,^{13,14} in an early attempt to understand hadron production in electron-positron annihilation. A QCD mechanism called *colour pre-confinement* occurring toward the end of the QCD shower evolution prompts colour neutralization into singlet *clusters* or resonances, that subsequently decay quantum mechanically onto the hadron/resonance mass spectrum. This decay is governed by phase space weights (Fermi Golden Rule), thus the outcome appears to be born into equilibrium, a maximum entropy state preserving the initial quantum numbers and the size of available phase space, represented by temperature and baryochemical potential in the Gibbs ensemble. Indeed the hadron multiplicities from e^+e^- annihilation can be well accounted for by the SHM. We show in Fig.1 the LEP data at 91.2 GeV confronted with the canonical SHM,¹⁵ revealing a hadronization temperature of 160 MeV. It agrees with Hagedorn’s limiting hadronic temperature as was predicted, already in 1975, right with the discovery of QCD, by Cabibbo and Parisi.¹⁶ The second line of argument concerning hadronization equilibrium stems from the recent idea¹⁷ to investigate the overlap between the Hadron Gas Model and lattice QCD with regard e.g. of the energy and entropy densities as a function of temperature.

4 Reinhard Stock

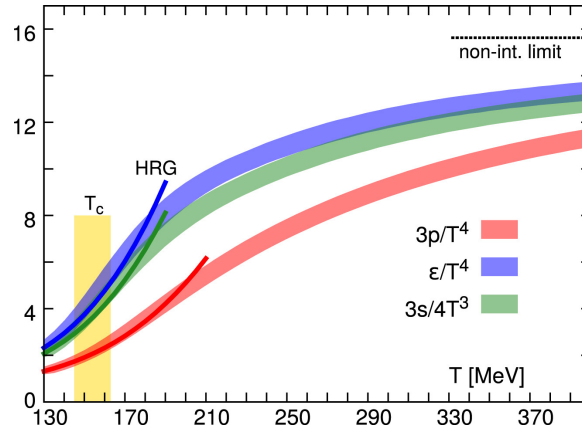


Fig. 2. Lattice QCD calculations for energy density and other quantities, confronted with Hadron-Resonance Gas model predictions for the same quantities.¹⁸

An example¹⁸ is shown in Fig.2 where we see the HRG curves intersect with the respective Lattice predictions in the vicinity of 165 MeV. I.e. below this temperature the degrees of freedom of an equilibrium HRG appear to take over from the lattice proper degrees of freedom. Note that the HRG and the SHM refer to the same hadron/resonance partition functions.

Next, we note that the results and predictions of lattice QCD are *exact* (in the sense of the model) only at zero baryochemical potential where the phase transition is a rapid cross-over. Toward finite μ_B various extrapolations are employed,^{2,3} for example a Taylor expansion¹⁹ the coefficients of which are, in fact, related to experimentally accessible higher order fluctuations of conserved quantities like baryon number and charge.^{20,21} We shall return to this work later on but note, for now, that an interesting feature of the emerging phase boundary line at finite μ_B would be the intensely discussed critical point of QCD,^{22,23} at which the crossover nature of the parton-hadron transition would end giving way to a first order transition toward higher μ_B . This would mark, on the one hand, the end of the lattice Taylor expansion, by divergence, but on the other hand lead to measurable changes in the sequence of hadronization points²³ which are accessible via SHM analysis of the hadronic multiplicity distributions. This analysis could, therefore, not only ascertain the much debated existence of a critical point, but also serve to locate the phase transition line toward higher μ_B where lattice QCD is inapplicable, as of yet.

The arguments above tacitly assume that the nucleus-nucleus collision dynamics does indeed cross the phase transformation line, and settles above it before re-expansion of the hot and dense matter volume sets in, to approach the phase boundary. I.e. that we are at collisional energies above the so-called “onset of deconfinement”.²⁴ Estimates of the corresponding incident energy domain (in central, heavy nuclear collisions) remain uncertain at present, pointing to the \sqrt{s} region from about 4 to 8 GeV. Below this (yet to be determined) energy the hadronic multi-

plicities would not stem from the QCD hadronization phase transition, which is responsible for the hadro-chemical equilibrium among the species' abundances.^{4,5,9–11} Thus, unless another phase transition comes into play at high baryochemical potential,²⁵ we should expect observable changes in the hadronic freeze-out pattern, such as a sequential chemical freeze-out in inverse order of inelastic cross section (characteristic of a diluting hadron gas). We shall return to this question at the end of this article but state, for now, that we can not yet arrive at clearcut conclusions concerning such features, due to a lack of data in the AGS energy domain, and below.

Turning to another important assumption of the above overall model considerations it was shown^{26,27} that the simple picture of an instant, synchronous chemical freeze-out of all hadronic species, occurring directly at the hadronization phase transformation, requires some revision. Final state inelastic or annihilation processes need consideration owing to the high spatial particle density after hadronization. This effect is perfectly absent in elementary collisions such as e^+e^- annihilation to hadrons where hadrons are born into the physical vacuum. The SHM was initially developed for such elementary collisions.²⁸ Turning to $A + A$ collisions it was shown that a detailed investigation of final state modifications of the multiplicity distribution exhibits relatively weak effects on the bulk meson production, pions and kaons which embody more than 90% of the total hadronic output energy at the LHC energy, but is important via annihilation of baryons and antibaryons, notably p and $pbar$. These effects were quantified using the microscopic transport model UrQMD, in its so-called *hybrid* version²⁹ where a hydrodynamic expansion mode of the collisional volume is terminated by a simulation of the hadronization process via the Cooper-Frye mechanism. The emerging hadrons and resonances are then traced through the ensuing, final hadron-resonance cascade expansion phase of UrQMD, and its attenuating effects can thus be determined, species-wise. These final state modifications affect the outcome of the SHM analysis as we shall demonstrate in the next section; they need to be taken into account before concluding on the position of the QCD phase boundary line. Beyond studying the changes occurring in baryon and antibaryon multiplicity, and their effects on the Statistical Hadronization model analysis^{26,27,30} as further discussed below, other groups have also focused on the consequences of this final state annihilation for the hydrodynamic, notably the elliptic flow of various identified hadronic species.³¹

In the next section we shall discuss an approach to overcome the final state effects, by generating UrQMD-modification factors for the hadronic multiplicities that lead to a modified SHM analysis. Turning to SHM analysis of data at LHC, SPS and AGS energies in Sec. 3 we discuss the resulting new freeze-out curve³⁰ and its differences to the result of a *standard* SHM analysis, as well as to the often quoted smooth interpolation curve given by Cleymans *et al.*³² In Sec. 4 we compare to the lattice QCD results for the parton-hadron phase boundary, confirming the lattice prediction^{2,3} that the line is almost horizontal up to a rather high μ_B . We

then turn to a discussion of the apparent tension between the SHM conclusion that $T_c = 164 \pm 5$ MeV and the recent conclusion from consideration of data, HRG and Lattice QCD results concerning higher order fluctuations of proton and charge multiplicity distributions, that appear to favour a lower transition temperature, of about 150 – 155 MeV.³³ Section 5 will give a short presentation of the issues concerning the SHM, i.e acceptance and stopping power effects, the core-corona model, canonical strangeness suppression, and new LHC $p + p$ collision results. A discussion section will end the paper in Sec. 6, where we will briefly return to the issues of critical point, and onset of deconfinement.

It remains to say that we will not re-iterate the theoretical formulation of the grand canonical Statistical Hadronization model in this brief overview. Comprehensive presentations can be found in references.^{4-6,8}

2. UrQMD final state effects and the Statistical Model analysis

Combined microscopic-macroscopic models are among the most promising approaches to describe nucleus-nucleus collisions.³⁴ Initial state effects causing event-wise fluctuations of the dynamics can be installed and investigated separately, as is the case for the study of the ensuing hydrodynamic flow expansion, and for the matching to the final state hadron-resonance cascade that leads to decoupling. The latter aspect is our concern here.

In the hybrid UrQMD model employed^{26,27} to assess the final state effects on hadronic multiplicities in $A + A$ collisions, the hydrodynamic stage is a full (3+1) dimensional ideal hydro model executed by the SHASTA algorithm,³⁵ employing the CH EOS from Ref.³⁶ which corresponds to a crossover transition from a hadronic gas to the QGP at $\mu_B = 0$ that extends to the region of finite μ_B , relevant for all beam energies discussed, at present. The hydrodynamic evolution was stopped, generally speaking, once the energy density (temperature) in the system falls below a pre-set critical value. Then the Cooper-Fry equations were sampled on a defined hypersurface, in accordance with conservation of all charges as well as the total energy. Two different choices of the hypersurface have been employed in order to assess the sensitivity of the ensuing *afterburner* effects to the initialization procedure. The first choice was an effective iso-proper time hadronization,³⁷ implemented by freezing out in successive transverse slices, of thickness $dz = 0.2$ fm, whenever the last flow cell of the considered slice fulfills the freeze-out criterion: an energy density ϵ below five times the nuclear ground state energy density (i.e. about 750 MeV/fm³). This procedure was carried out separately for each slice, and the particle vector information transferred to the cascade part of the UrQMD model.²⁹ The effect of final state interaction was then quantified by either stopping the calculation directly after hadronization, letting the produced hadronic and resonance species undergo all their strong decays as if in vacuum, thus establishing a fictitious multiplicity distribution ideally referring to the hadronization *point*. Alternatively, the final afterburner UrQMD stage was attached, and the multiplicity distribution

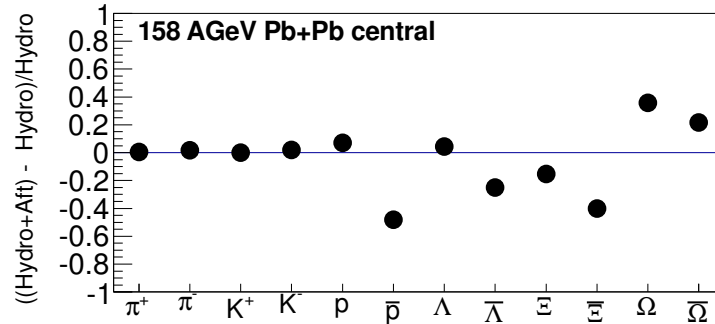


Fig. 3. Modification factors accounting for final state attenuation in the hadron/resonance expansion.^{26,27}

at decoupling generated. For each hadronic species one could then extract a modification factor indicating the strength of the afterburner effects (a method introduced by Bass and Dumitru³⁴). This factor got finally employed in the SHM analysis of the data (see Sec. 3).

In a further investigation³⁰ an alternative choice of the hadronization hypersurface was explored, corresponding to an isothermal termination of the hydro expansion stage of UrQMD. Here, one implements the switch to hadronic/resonance degrees of freedom locally, in each hydro-flow cell, once it falls below the pre-set energy density, or temperature, calculating the hypersurface element with a state of the art hypersurface finder.³⁸

In the following we illustrate this overall procedure, and its main consequences as far as the UrQMD predictions for final state attenuation of hadronic abundances are concerned. The resulting modification factors are employed in the data analysis with the Statistical Hadronization Model (Sec. 3). For illustration of the phenomena we choose the case of central $Pb+Pb$ collisions at the top SPS energy, $\sqrt{s} = 17.3$ GeV (one of the data sets to be analyzed in Sec. 3). Figure 3 shows the modification factors²⁶

$$M = \frac{yield(\text{with afterburner}) - yield(\text{at hadronization})}{yield(\text{at hadronization})} \quad (1)$$

for the hadronic species covered by the experiment. One sees the pion, kaon, proton, Lambda and Xi yields, i.e. the bulk output from hadronization, to be essentially unaffected at this incident energy, a remarkable result. Thus far the assumption of a synchronous freeze-out, directly at hadronization, as made in the standard version of the SHM,⁴⁻⁷ is substantiated. On the other hand, antiprotons suffer a net loss of about 50%, and Anti-Lambda and Anti-Xi multiplicities are reduced by 25 to 40%. The Omega/Anti-Omega hyperons are less affected because they have no excited resonant states, and freeze out from the cascade evolution almost instantaneously, owing to their low total cross section. There may also occur contributions of baryon/antibaryon regeneration³⁹ which are only partially implemented

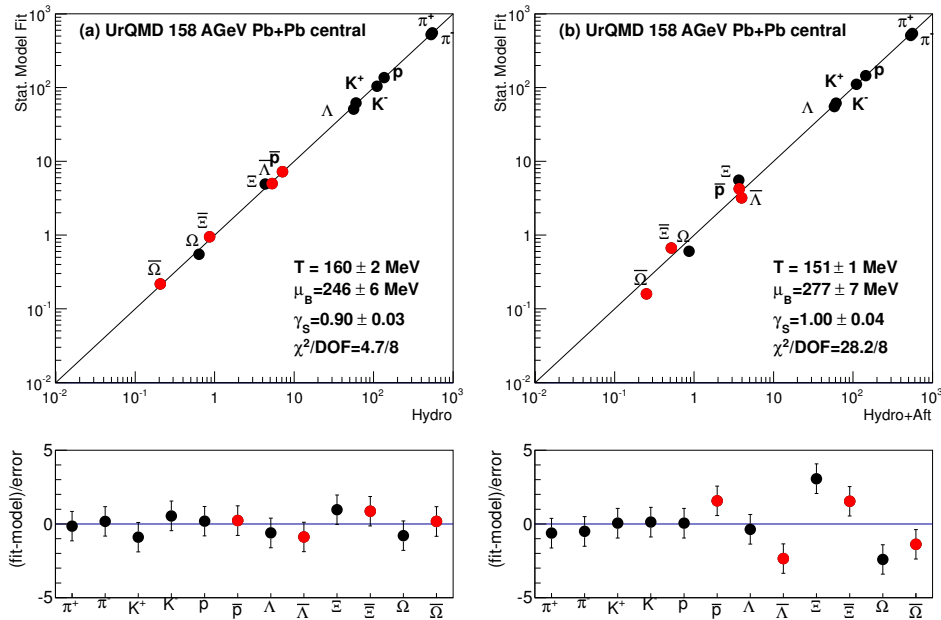


Fig. 4. UrQMD multiplicities fitted by the Grand Canonical model, fitted to the “data” right after hadronization, and to the results with attached UrQMD afterburner.²⁶

in UrQMD. A new study of their importance is under way with the QHDS transport model.⁴⁰

We see that in the UrQMD cascade evolution inelastic reaction channels are of no major importance whereas baryon-antibaryon annihilation channels do not freeze-out directly after hadronization. At the relatively low SPS energy, illustrated here, baryons are far more abundant than their anti-partners; thus their partial annihilation with antibaryons changes a minor fraction of their multiplicities, whereas the antibaryons are significantly diminished, fractionally. This pattern changes at LHC energies due to the near-perfect particle-antiparticle symmetry, prevailing there.²⁷ Under such conditions the antibaryons are equally affected.

These attenuations have a profound effect on the Statistical Model analysis. The loss of antibaryons is, clearly, a departure from the initial chemical equilibrium distribution which is reflected in a SHM analysis (described in Ref.²⁶) of the two sets of UrQMD multiplicities, obtained with, and without the afterburner stage.

This is shown in Fig.4: the UrQMD multiplicities, taken as “data”, have been fitted with the SHM. We see that, on the one hand, the SHM fit to the no-afterburner results is of excellent quality and reveals a hadronization temperature of 160 MeV. This is not surprising because the SHM fit merely responds to the chemical equilibrium multiplicity distribution imprinted by the Cooper-Frye hadronization, with its preset temperature value. On the other hand, the case with afterburner shows

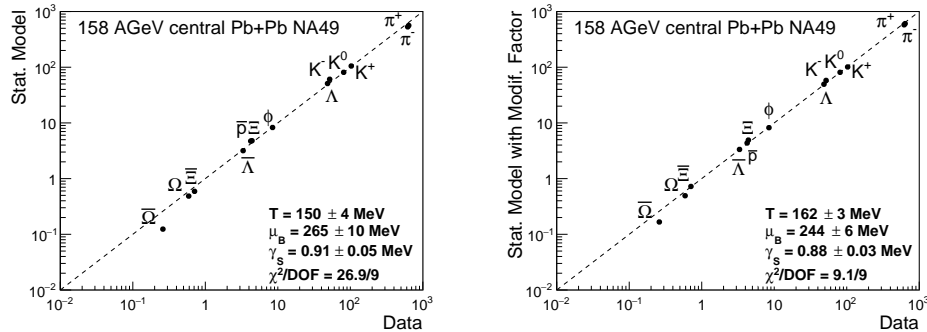


Fig. 5. Hadron multiplicities from central $Pb + Pb$ collisions at top SPS energy, confronted with HRG fits employing the standard Grand Canonical approach, and the SHM corrected by UrQMD modification factors.²⁶

a very much deteriorated fit in the antibaryon sector, at a temperature reduced to 151 MeV. The apparent chemical freeze-out temperature thus drops down, significantly, due to the final state distortions of the multiplicity distribution. The traditional statistical model analysis thus needs revision. We will show this in the next section, turning to data analysis.

3. Data Analysis: the SHM Freeze-out Curve

In this section we illustrate the UrQMD-modified Statistical Model analysis³⁰ that addresses 5 hadronic multiplicity data sets obtained, respectively, by ALICE⁴¹ at the LHC energy of 2.76 TeV per nucleon pair, by NA49⁴² at the SPS energies 17.3, 8.7 and 7.6 GeV, and by the AGS experiments E891, 802, 896, 877⁴³ at 4.85 GeV. All data refer to central collisions of $Au + Au$ (at the AGS) and $Pb + Pb$ (at SPS and LHC). Note that the new STAR data⁴⁴ from the RHIC BES program have not been included in this analysis because they are not yet corrected for antiproton feed-down from secondary weak antihyperon decays. In Fig. 5 we illustrate this analysis choosing the case of the top SPS energy data, central $Pb + Pb$ collisions at 17.3 GeV. The outcome of the *traditional* SHM analysis⁶ is compared with the version in which the SHM fit to the data is done with theoretical multiplicities modified by the final state attenuation factors from UrQMD (see Fig.3). Two major effects are obvious: the deduced temperature increases significantly, from $T = 150$ MeV in the former, to $T = 162$ MeV in the latter case. Concurrently, the fit chi-square/dof drops dramatically, from about 2.7 to about 1.0. The UrQMD-reconstructed yield distribution, which aims to re-establish the distribution at hadronization, obviously meets with the grand canonical equilibrium hypothesis, implicit in the SHM approach. Recalling the analogous observations derived above, from the SHM study of UrQMD predictions for the multiplicity distribution (Fig.4), we re-iterate the conclusion that the final state hadron/resonance cascade evolution (here represented by the UrQMD *afterburner*), generates a distortion of the hadro-chemical equilibrium

yield distribution that is initially imprinted at hadronization. This is reflected in the unsatisfactory SHM fit quality, a feature also reported from the SHM analysis of Andronic *et al.*¹²

A short remark is in order here, to clarify the above use of the term equilibrium. First, it refers, not, to a global equilibrium of all aspects of the phase space distributions of the hadrons that emerge from the QCD hadronization phase transformation. It refers, only, to its first moment, the hadronic yield (multiplicity) distribution. Higher moments, such as collective, discrete hadron emission flow patterns (radial, directed, elliptic and higher flow orders) represent non-isotropic momentum space flow moments at any higher order, in the final state. Furthermore, if the hadronization process creates a hadronic species thermal equilibrium distribution (which is represented by the quasi-classical equilibrium grand canonical Gibbs ensemble underlying the Statistical Model) directly corresponding to the conditions prevailing at hadronization (chiefly the energy density/temperature), this equilibrium state, if it freezes-in directly at this point (as assumed in the traditional SHM analysis), is of course out of equilibrium immediately after the onset of expansive dilution and cooling. The yield distribution does, ideally, not adjust to the falling energy density but stays, frozen into the ongoing expansion, as we have seen in Fig.3, to appear as the bulk hadronization output. The hadron/resonance expansion stage will adjust other, higher moments. We note that also the higher moments of conserved baryon number and charge multiplicity fluctuation may not become stationary (freeze out) at the very instant at which the number and entropy densities of the hadron/resonance degrees of freedom get fixed. We shall return to this consideration below, when discussing the recent work on fitting kurtosis and skewness data, and HRG predictions, to the corresponding results from lattice QCD. Thus there are two, or perhaps even three successive freeze-outs: the primordial hadronic species distribution reflects the energy/entropy densities prevailing at the onset of hadronization (with corrections that this study quantifies) whereas higher order multiplicity fluctuations may be imprinted throughout the duration of the hadronization period (which is finite in a cross-over transition). Finally, spectral and correlation features become stationary at the lower temperatures of decoupling from all strong interaction(kinetic freeze-out).

The results from Ref.³⁰ concerning the reconstruction of the hadronization line, in the plane of temperature T and baryochemical potential μ_B are summarized in Fig. 6. It shows the (T, μ_B) points at the 5 energies considered here, that result from SHM analysis of the corresponding hadron multiplicity data sets. The results of the standard SHM approach are compared to the UrQMD-modified SHM in both the hadronization modes described in Sec. 2, isothermal and slice-by-slice. The latter give almost indistinguishable results pointing to the conclusion that the detailed method employed for UrQMD hadronization has little influence on the effects of the ensuing cascade expansion stage, as far as multiplicities are concerned. Up to a baryochemical potential of about 370 MeV the points exhibit very little downward

slope, unlike the results from standard SHM analysis which drop off more steeply. This invites comparison to the lattice QCD predictions for the curvature of the phase boundary line, a subject of the next section, as is the apparent abrupt downward turn toward higher μ_B (unfortunately documented by a solitary AGS point only). As far as the turn-off toward higher baryochemical potential is concerned, which may indicate the advent of new physics as discussed in the next section, we note here that this feature has been well recognized already in previous investigations of the SHM freeze-out, which did not employ any final state attenuation corrections. We show in Fig.7 the state of the art as of 2006 by reproducing the results obtained by Andronic *et al.*⁷ for the SHM freeze-out systematics as function of μ_B , gathering all results available at that time. Indeed, the authors note that the turn-off, corresponding to SHM investigations below a CM energy of about 8 GeV, is hardly compatible with any smooth interpolation.

Finally, we note here that the much discussed puzzle^{12,41} of an apparent *non-thermal*, high pion to proton ratio observed in the ALICE data⁴¹ at the LHC energy of 2.76 TeV (which resulted in an unsatisfactory SHM fit¹²) finds its resolution in the UrQMD modified approach illustrated above. Final state annihilation of nucleons and antinucleons reduces the p and pbar multiplicities while increasing the pion yield as each annihilation contributes 5 pions, on average. Both the p, pbar losses, and the additional pion gains are, of course, of non-thermal origin.

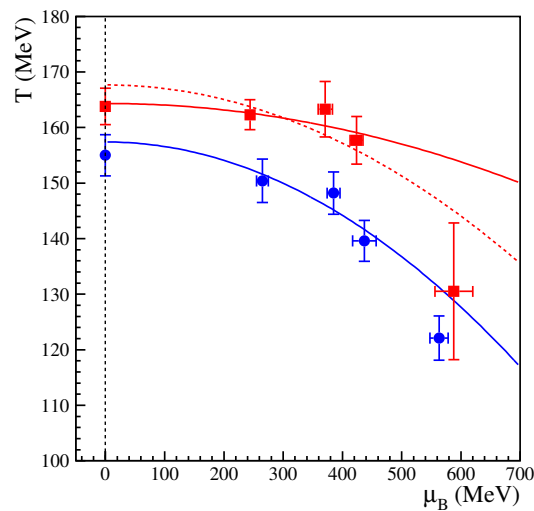


Fig. 6. Results of the UrQMD plus SHM approach, for hadronization points in the (T, μ_B) plane. The lower set of points represents a standard grand canonical SHM analysis.³⁰

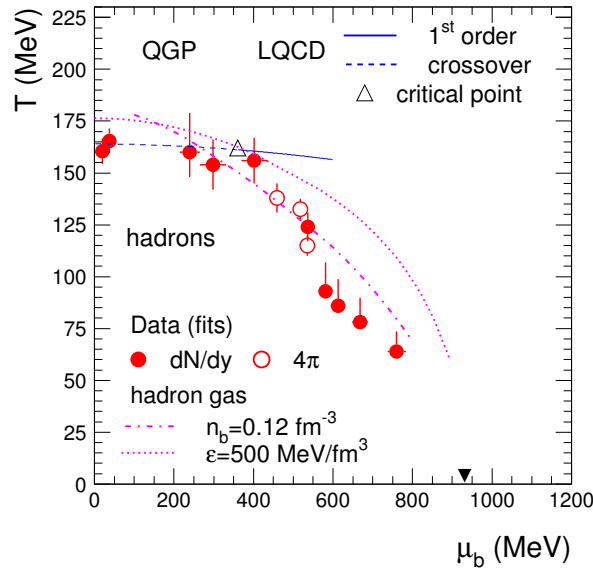


Fig. 7. Standard SHM analysis results for freeze-out points in the (T, μ_B) plane, covering energies from RHIC, via the SPS and AGS, down to SIS18.⁷

4. Comparison to Lattice QCD

We wish to discuss, in more detail, the observations described above.

- (a) The small initial slope of the UrQMD modified SHM model points resembles the recent lattice predictions for the QCD transition line^{2,3} which employ a quadratic ansatz,

$$T_{c,\mu_B} = T_{c,0}(1 - \kappa_{2,B})(\mu_B/T_{c,0})^2 \quad (2)$$

reporting curvature values $\kappa_{2,B}$ between 0.007 in Ref.² and 0.015 in Ref.³ The first 4 points are compatible with $T_{c,0} = 164$ MeV and $\kappa_{2,B} = 0.0048$.

- (b) The steep drop-off in the μ_B domain above about 400 MeV may represent a manifestation of a fourth order coefficient $-\kappa_{4,B}(\mu_B/T_{c,0})^4$ in the lattice Taylor expansion. This, then, would be of order 0.003 but we note that this estimate is based on a single data point (AGS) only. We can not decide, with certainty, whether the QCD phase boundary moves downward, steeply, in this domain. Alternatively, the steep drop-off could signal a change in the collisional evolution, such as the advent, at high μ_B , of the hypothetical quarkyonic matter phase²⁵ interpolating between the domains of deconfined, and of hadron-resonance matter in the QCD phase diagram, thus shifting the final hadronization transition downward in temperature.

Hadronization from a quarkyonic matter phase has not yet been considered theoretically so that we can not say with certainty that it would feature a similarly phase space dominated yield distribution over species. Finally, and more simply, we might witness the so-called “onset of deconfinement”²⁴ at the AGS energy, where the collisional volume does deconfine only partially, thus lacking a phase transition synchronized hadronic freeze-out.

- (c) Obviously, the reconstructed hadronization points in Fig. 6 indicate a (pseudo-)critical temperature $T_{c,0}$ of 164 ± 5 MeV, at $\mu_B = 0$ and, likewise, a T_c above about 160 MeV in the entire μ_B interval up to about 370 MeV. This observation is, clearly, at odds with the recent consensus in lattice QCD studies about a lower $T_{c,0}$ value, in the vicinity of 150 to 155 MeV.³³ However, let us not rush for conclusions here. As we said above, higher order fluctuations (susceptibilities) might freeze out later than the zero-order multiplicity quantities (their overlap with lattice QCD thus occurring at a lower T) and, moreover, they might not be reliably accounted for by the noninteracting HRG model due to attractive short range interactions.⁴⁵ Thus the HRG-Lattice overlap temperature, as derived from the fluctuation/susceptibility observables, may not be a good approximation of $T_{c,0}$. Finally we recall that Fig. 2 did suggest a $T_{c,0}$ above 160 MeV from state of the art lattice calculations for the equation of state and the energy density — the quantities more closely related to hadron/resonance number density (that is of relevance in the SHM and also, of course, in the HRG) than e.g. the Polyakov-loop slope turnover, or higher susceptibilities. Addressing the former observables the HRG-lattice overlap region rather suggested a $T_{c,0}$ above 160 MeV.
- (d) The UrQMD-modified results represent a revision of the *hadronic freeze-out curve* that was obtained³² by an interpolation of the (T, μ_B) values deduced from grand canonical SHM analysis of central $A + A$ collisions, gathered from RHIC energies down to AGS and SIS18 energies.⁴⁻⁷ This often shown curve also extrapolated to a $T_{c,0}$ of about 165 MeV. However, the various sets of hadron multiplicity data, available by 2006 for AGS, SPS and RHIC energies, had mostly not yet been corrected for experimentally unresolved feed-down contributions stemming from weak decays of the hyperons/antihyperons. This increased the apparent multiplicities for baryons/antibaryons, reflected, in the SHM analysis, by too high temperature assessments. The data sets used in Fig. 6 are properly corrected, thus the corresponding standard freeze-out curve moves below the 2006 result, by about 10 MeV as shown in Fig. 3. We note that, anyhow, this standard SHM result loses interest due to the annihilation processes in the final cascade evolution, which have, first of all, to be accounted for, by an analysis like the one described above. Whether or not the particular UrQMD approach represents the last word about this issue clearly remains to be clarified.

5. Issues of Concern in SHM Analysis

Let us begin this chapter with a general observation. The consistency of existing SHM analyses suffers from the plurality concerning details of the employed analysis formalism or, even, its basic formulation. We shall take up some such aspects in some more detail below but mention, for now, the options for or against e.g. hadron eigenvolume corrections, strangeness correlation volumes or a strangeness fugacity, corona-core separation, light quark fugacity, to name just a few. Furthermore, the available data reflect different experimental acceptance conditions (both in rapidity space and in azimuthal coverage), and data sets comprise a varying sub-selection of hadronic species, the latter often a consequence of hyperon multiplicities falling strongly with incident energy. Thus, a set of multiplicities ranging from pions up to anti-Omega hyperons gets employed from LHC down to top SPS energies, but the rarer species fall away, gradually, toward lower energies. This is counterproductive if one tries to secure a systematic coverage of the overall T, μ_B dependence. Overall, we note that the ideal view represented by the standard grand canonical ensemble may not be universally congruent to the reality of $A + A$ collisions,⁶ and of their measurement within certain fixed rapidity windows (see below). Thus the data sets of multiplicities may reflect *tensions* that vary with energy; the acceptance problem, for example, disappears only with approaching boost invariance, i.e. at top LHC energy. And the annihilation corrections affect, significantly, only the antibaryons at low energy because of the large excess of B over Bbar. Whereas both B and Bbar are attenuated at high energies.

Numerous further SHM analysis problems can be enumerated. An example is the question of how to treat the Phi-meson: with strangeness suppression (creation from $K^+ - K^-$ pairs) or without (strangeness zero at hadronization). A further, new question: should the charmed hadrons be included in the general SHM fit (with a special fugacity factor as charm is not thermally produced), or should we expect a sequential hadronization of the heavier quarks⁴⁶? We shall take up some of such questions below but end here showing a fairly complete selection of available standard SHM analyses,⁴⁷ from LHC down to SIS18 energies, in Fig. 8.⁴⁸ Quite expectedly the points exhibit considerable dispersion even though the results with UrQMD modification (Fig. 6), and the predictions of the Single Freezeout Model⁴⁸ have not been included here.

5.1. Acceptance and stopping power effects in rapidity space

The thermal rapidity spreading width of a single midrapidity fireball is proportional to $(T/m)^{1/2}$ for a hadron species of mass m .⁴⁹ For pions emitted at $T = 160$ MeV this amounts to the interval $-1.3 < y < 1.3$, whereas emitted Omega hyperons would occupy a much smaller interval, of about $-0.4 < y < 0.4$. Kaons fall in-between. Realistically, a fireball of 160 MeV temperature could get created at top SPS energy (recall Fig. 6), but here it features, in addition, collective radial

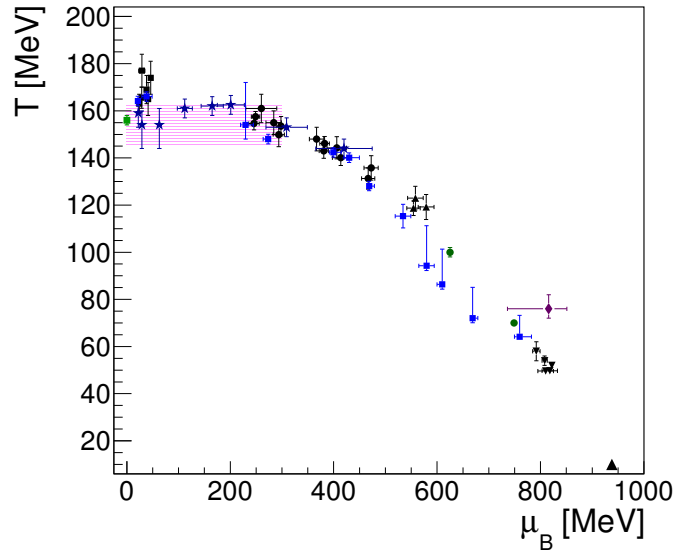


Fig. 8. Summary plot of present SHM analysis with various variants of the Statistical Hadronization Model, for the overall freeze-out curve in (T, μ_B) space.^{46,47}

flow expansion which elongates the longitudinal rapidity distributions.⁵⁰ The pions thus acquire a width of about ± 1.5 units of rapidity whereas all heavier hadrons stay within an interval of unit rapidity. This is the STAR experiment acceptance, employed in the BES RHIC runs at low energy, down to the SPS regime where considerations such as above may be realistic. Such an acceptance thus creates an artificial strangeness enhancement, as reflected in the so-called Wroblewski ratio.⁵¹ It counts the total number of s and \bar{s} quarks, relative to the light quark number, recovered in the observed hadronic multiplicities. The pions that carry the major fraction of the light quarks partially leak out of the narrow acceptance. This creates *tensions* in the SHM analysis.

A remedy might be to widen the experimental acceptance. The resulting effects can be studied with data from fixed target experiments, such as NA49 at the SPS, and BRAHMS at RHIC. The former already reported a minimum at midrapidity in the net baryon rapidity distribution for central $Pb + Pb$ collisions at 17.3 GeV c.m. energy.⁵² This signals a minimum of the baryochemical potential which, in turn, is a consequence of the so-called stopping power of hadronic matter. The net baryon number density reflects the final distribution, in longitudinal phase space, of the valence quarks carried in by the colliding nuclei. In a Glauber-like picture the transport of valence quarks, from initial target/projectile rapidity positions inward toward midrapidity occurs via the successive binary collisions of nucleons (or their remnants) during the primordial interpenetration phase, which extract partons from the initial nucleon structure functions. This stopping mechanism

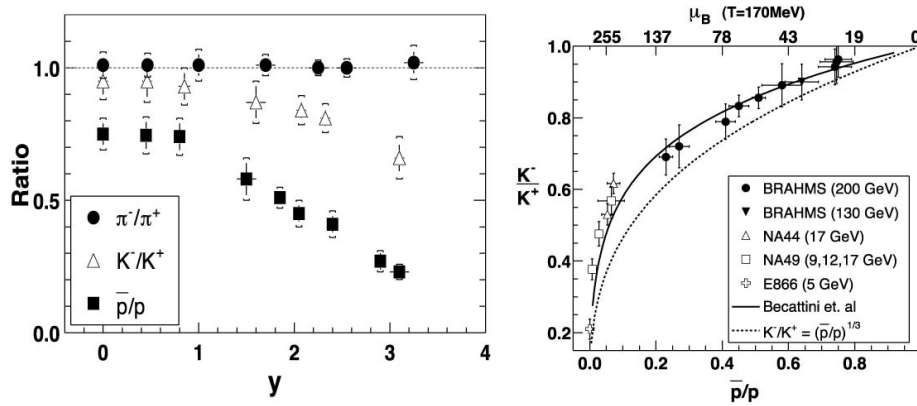


Fig. 9. Results of the RHIC BRAHMS experiment⁵³ for antihadron to hadron ratios at top RHIC energies. The left panel shows the rapidity dependence, the right confronts a correlation plot of K^-/K^+ vs. \bar{p}/p with SHM calculations at constant temperature but with decreasing baryochemical potential.

spreads the bulk of the valence quarks over about 2.5 units of rapidity in central mass 200 nuclear collisions. From top SPS energy onward, the rapidity gap between the initial target and projectile rapidities, increases beyond $dy = 6$, and the midrapidity region is increasingly devoid of valence quarks, thus μ_B falls toward zero here. This can be perfectly illustrated by the BRAHMS results⁵³ shown in Fig. 9. The left panel shows results for central $Au + Au$ collisions at 200 GeV, exhibiting the rapidity dependence of the multiplicity ratios π^-/π^+ , K^-/K^+ and \bar{p}/p . The latter two are proportional to $\exp(-2/3 \mu_B/T)$ and $\exp(-2 \mu_B/T)$, respectively, thus presenting a direct measure of μ_B . Obviously this stays near constant within $0 < y < 1$, the heavy hadron radiation width as argued above. However, a different physics seems to set in, in each successive further unit rapidity interval. No use in widening the acceptance in a SHM analysis that seeks to establish the prevailing (T, μ_B) point in the phase diagram, because μ_B increases, steeply, toward higher y where the valence quark density increases.

This is further demonstrate in the right panel of Fig. 9 where the correlation between K^-/K^+ and \bar{p}/p is confronted with an interpolating SHM fit curve. The inferred μ_B shifts down from the 20 MeV domain, corresponding to a relatively valence quark free midrapidity domain, to about 140 MeV, smoothly interpolating, furtheron, to data points from the SPS domain.

To conclude about our above question of increasing the acceptance to secure the true Wroblewski ratio we see that from top SPS to top RHIC energies this is not helpful because each successive unit rapidity window reflects a differently composed hadronization source. This is the consequence of the hitherto little explored stopping mechanism that governs interpenetrating hadronic matter. At top LHC energies, the valence quark domain recedes far from midrapidity, and the acceptance is of no concern in this domain where μ_B is practically zero, and T is constant (boost

invariance). At low energies, on the other hand, the rapidity gap is so small that the energy and quark distributions fall mostly within a single fireball radiation width: conditions yet to be explored in detail.

5.2. Core-Corona effects and canonical strangeness suppression

Glauber model calculations reveal that, even in central collisions, a small fraction of the target and projectile nucleons does not interact, at all, and a further about 10% fraction of the participant nucleons interacts only once. Toward peripheral collisions that latter fraction increases toward about 25%. These single, minimum bias nucleon-nucleon collisions exhibit canonical strangeness suppression.^{6,8} The Wroblewski ratio of total strange to total nonstrange quarks in $p + p$ collisions is half that in central mass 200 $A + A$ collisions.⁵⁴ In the SHM the transition from $p + p$ to $A + A$ occurs as a change-over from a canonical to a grand canonical ensemble that occurs, gradually, with increasing N_{part} .^{6,8} Singly strange/antistrange yields rise, by a factor of about two, relative to minimum bias $p + p$ at similar energy, and by factors of about 5 and 15, respectively, for multistrange hyperons.^{54,55} The single collision fraction of $A + A$ collisions stems from the diffuse surface regions of the nuclear Woods-Saxon nucleon density distributions. Thus one calls this the *corona effect*.^{6,54,56} It reduces the strange to nonstrange hadron yield ratios in $A + A$ collisions, as compared to a global grand canonical equilibrium population. One attempt to account for this strangeness undersaturation is to introduce a strangeness undersaturation parameter $\gamma(s)^S$ into the partition functions of the GC Gibbs ensemble;⁶ $S = 1, 2, 3$ here. This is thus an additional fit parameter, in addition to the GC variables V , T and μ_B . It is found to amount to about 0.85 to 0.90 in central mass 200 collisions at SPS and RHIC energies,⁶ increasing toward peripheral collisions.⁵⁷

We can illustrate a typical interplay between several such second order corrections to the standard GC approach. The effect of a narrow midrapidity acceptance (see previous section) is expected to lead to an increase of the apparent Wroblewski ratio whereas the corona effect decreases it. The net effect might be a cancellation and, in fact, it was shown⁶ that the NA49 data for central $Pb + Pb$ collisions at top SPS energy (referring to a wider acceptance, of about $0 < y < 2$ required a $\gamma(s) = 0.85$ whereas $\gamma(s) = 1$ as the SHM fit was restricted to a $0 < y < 1$ acceptance interval.

5.3. The origin of canonical strangeness suppression

We address, next, a qualitatively different strangeness undersaturation effect, that governs elementary electron-positron annihilation to hadrons, and minimum bias $p + p$ collisions.^{58,59} We have shown in Fig. 1 the canonical SHM fit to the LEP e^+e^- annihilation data. It requires another, further strangeness suppression factor, $\gamma(s) = 0.66$. Unfortunately the same term is used here as in the GC SHM

analysis of $A + A$ collisions, confusing the issue as this suppression is of completely different origin. It can be understood from the Amati, Veneziano, Webber^{13,14} model of colour neutralization in elementary QCD hadronization that we referred to in Sec. 4. Here the primordial QCD partonic shower evolution is shown to end in a string-like configuration of successive complementary colour charges that locally neutralize into colour singlet clusters, with varying invariant masses. They decay, independently, into hadrons and resonances, according to their respective phase space weights. The clusters are distributed over the entire longitudinal phase space, and thus they are, in general, not causally connected.^{58,59} However, as shown by Becattini and Fries,⁴ the Lorentz invariant single cluster multiplicities and net quantum numbers can be added into a single *equivalent global cluster*, whose volume is the sum of the proper individual cluster volumes, turning out to be large enough to make the canonical ensemble a good approximation.⁶⁰ However, the small volume, high microcanonical strangeness suppression (apparently due to the strange quark mass), prevailing in the individual cluster decays, gets transported into the equivalent global cluster strangeness content: a memory of the microscopic QCD dynamics leading to cluster formation. As the canonical SHM is ignorant of that microscopic pre-history it needs to be amended by an additional strangeness suppression parameter. It recalls that strangeness was produced in small, causally disconnected clusters, under high strangeness suppression.

From this, admittedly somewhat symbolic model, to hadron production from a QCD plasma, in $A + A$ collisions: how does a QGP hadronize? Clearly, the first stage of the above schematic model, local colour neutralization, has to be in common. We are not aware of any theoretical argument as to why this should not be a short-range, local process, imbedded into the overall collective expansion/cooling dynamics as the plasma approaches the critical or pseudocritical energy density domain. Furthermore it is plausible that the cluster density in phase space should now be about A times higher. So the phenomenon of isolated, single cluster hadronization that we addressed above under the symbolic term *causally not connected* should disappear, leading to a quantum number coherent large equivalent super-cluster decay, that is mirrored in the success of the Grand Canonical, large volume SHM description of the $A + A$ hadron output. As we have seen from the BRAHMS results in Fig. 9, such fictitious superclusters can not extend over all longitudinal phase space, as successive intervals in rapidity space reveal a GC hadronization under different (T, μ_B) conditions. But, on the other hand, the genuine small cluster volume strangeness suppression, known from elementary (minimum bias) collisions, has disappeared here, hinting at a much larger, coherent decay system, in accord with the above schematic super-cluster picture.

In all, the reader will notice, however, that we employ here a highly symbolic terminology. Clusters, and super-clusters, are not yet known from genuine QCD calculations. They may be understood as an extrapolation from the concept of massive hadronic resonances. However, the formal three-step idea may reflect, in a

minimal way, the three steps expected from fundamental QCD: colour neutralization corresponding to the confinement transition, hadronic (cluster) mass generation symbolizing QCD chiral symmetry breaking, and the final quantum mechanical decay into on-shell hadrons/resonances representing the final tunneling effect, with its intrinsic phase space dominance, a la Fermis Golden Rule, that makes the apparent hadro-chemical equilibrium plausible.

5.4. Onset of Grand Canonical hadron production at the LHC

It has been predicted, before the startup of the LHC, that at $\sqrt{s} = 7$ TeV the midrapidity production of hadrons in $p + p$ collisions might approach the grand canonical limit⁶⁰ of the SHM description. These expectations can now be checked with ALICE $p + p$ data⁶¹ on strangeness production vs. multiplicity density $dN(ch)/d\eta$. In the cluster-terminology employed in the previous section the advent of GC strangeness saturation would have to imply an increasing overlap (or *causal connection*) among the microscopic singlet clusters, in longitudinal phase space. Looking at the midrapidity densities of charged hadrons we find $dN(ch)/d\eta = 3.3$ in LEP electron-positron annihilation (Fig. 1), and 6.0 in minimum bias $p + p$ at 7 TeV. The latter value⁶¹ is quite in line with the $p + p$ systematics at lower energies.⁵⁴ As the former case did require the application of the strangeness suppression factor 0.66, characteristic of elementary collisions at such lower energies,⁶⁰ one would not expect a substantial, qualitative change in $p + p$ at the LHC as the cluster density increases by less than a factor of two. However, the ALICE data shown in Fig. 10 imply that, on the contrary, significant strangeness enhancement (the reversal of strangeness suppression) occurs, with increasing midrapidity charged hadron density. Of course in the highest multiplicity bin, analysed here, we have $dN_{ch}/d\eta = 21.3$, now in fact 6.5 times higher than in e^+e^- annihilation at LEP. Also the enhancement effect increases strongly with ascending strangeness, quite resembling the strangeness hierarchical increase in the course of a transition from the canonical to the grand canonical ensemble.^{8,54} However, we also see in Fig. 10 that the Omega to pi ratio, for example, grows by a further factor of about two, toward semi-central $Pb + Pb$ collisions at 2.76 TeV. As the latter reaction should represent full GC strangeness saturation, we finally conclude that, even in the high multiplicity density windows of $p + p$ at LHC, we see no fully developed GC behavior but the onset of it. A GC SHM fit to these data would thus feature a non-unity, genuine $\gamma(s)$ factor.

A final remark concerning $p + p$ data as a reference for hadron production in $A + A$ collisions, as expressed in the nuclear modification factor R_{AA} . Note that this is commonly defined as the ratio between $A + A$ cross section and the corresponding minimum bias $p + p$ cross section scaled with the number of binary collisions, corresponding to the considered $A + A$ centrality class. However, this ratio is only applicable at high transverse momentum, well above the domain of thermal bulk production. Here the hadron multiplicities scale with the volume of the emitting

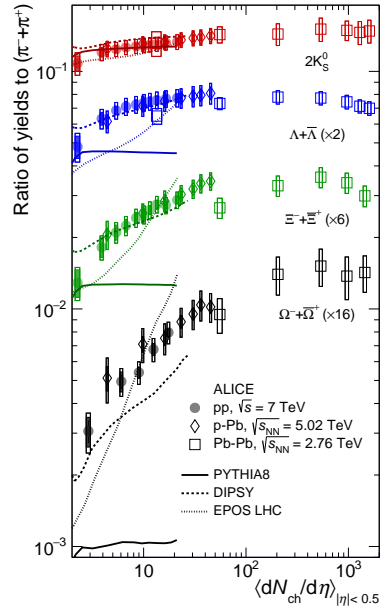


Fig. 10. ALICE results for $p+p$ collisions at LHC energy, $\sqrt{s} = 7$ TeV,⁶² showing the multiplicity dependence of strange hadron to pion yields, matching to results from $p+Pb$ and $Pb+Pb$ collisions.

source, proportional to N_{part} , and not with the Glauber binary collision number that increases like $N_{part}^{4/3}$. At high p_t there should be no problem with employing R_{AA} .

6. Conclusions

The fundamental interest in Statistical Model analysis stems from the hypothesis that the derived freeze-out points in the (T, μ_B) phase diagram should, at modest μ_B , coincide with the QCD hadronization points, thus revealing the parton-hadron transformation line of QCD: one of the principal characteristics of thermal QCD, in the non-perturbative domain. It was the purpose of this article to demonstrate that SHM studies are converging toward this goal. One needs, however, to take care of numerous second order concerns in the application of the grand canonical SHM. From among these, we have addressed final state annihilation corrections, experimental effects stemming from lack of feed-down corrections arising from unresolved, secondary vertex weak hyperon and antihyperon decays, and proper handling of acceptance and core-corona effects. Further problems require attention, such as finite hadron volume corrections⁶² and the clarification of the relationship between the SHM and coalescence model approaches.^{4,63} Finally the validity of the single freeze-out model^{8,47} still awaits a clarification. Turning to the idea¹⁷ to replace, or substitute the traditional SHM analysis by considering the overlap between Lattice

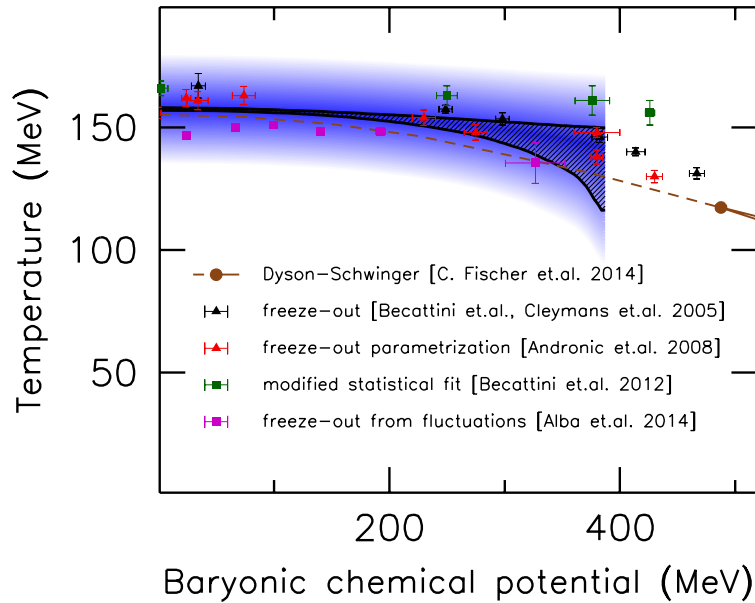


Fig. 11. The QCD phase diagram at finite baryochemical potential showing the domain of the crossover transition, confronted with various entries from SHM and Dyson-Schwinger analysis(see Ref.⁶⁶ for detail).

QCD and Hadron-Resonance-Gas(HRG) model calculations: this should provide for an alternative method to locate the (pseudo-)critical temperature domain over which partonic degrees of freedom convert to the hadronic ones.¹⁸ One can also analyze, directly, the first data concerning higher order grand canonical fluctuations of conserved quantum numbers, such as skewness and kurtosis, in terms of Lattice predictions for higher order susceptibilities.^{19,20,33,64} We have argued that not all of the various quantities, addressed in this framework (to which we could only provide a passing glance), should necessarily reveal a common freeze-out temperature,⁶⁵ given the broad band of temperatures encountered in a cross-over phase transformation as is encountered at modest μ_B . First order quantities, like energy and entropy densities (closely related to the hadron number densities considered in the SHM), might freeze out sooner than fourth order susceptibilities. Finally the Hadron-Resonance Gas approximation to the latter type of quantities may lack validity.⁶² To wrap up on this new research field, of HRG-Lattice QCD-data analysis,

and also the recent attempts in Lattice QCD to pin down the pseudo-critical line (or domain) in the QCD phase diagram, we show in Fig. 11 the result of a recent study of the phase diagram, by Bellwied *et al.*⁶⁶ The relatively broad domain of the cross-over transition in the (T, μ_B) plane, reaching up to limit of validity of the employed extrapolation method for finite μ_B domains, at about 400 MeV, is shown to envelope individual entries stemming from SHM and other approaches (see Ref.⁶⁶). We conclude that a detailed description of the QCD parton-hadron transition, far into the finite μ_B domain, appears within reach now, a formidable task commensurate to its fundamental importance. What remains, relatively much less explored, is the high μ_B domain. A rather abrupt turn-over occurs⁷ at a μ_B of about 400 MeV, but the scarcity of data in this domain prevents us from answering several interesting questions concerning the high μ_B domain:

- (1) If one considers the lattice extrapolations to apply, at all, to such high μ_B we might ascribe the the steepening slope to higher than quadratic terms in the lattice Taylor expansion.
- (2) If the enigmatic critical point of QCD exists, at all, it should occur¹⁶ at high μ_B , and influence the sequence, and position of the hadronization points (their dependence on the incident energy of the collision). This might occur, either, due to the onset, at the critical point, of a first order phase transition, or to the hypothetical focusing effect on the systems expansion trajectories.¹⁷
- (3) A further untested suggestion would explain the rather steep fall-off toward AGS energy. If the so-called quarkyonic matter domain of QCD¹⁹ exists, and sets in at the temperature of the critical point, one would expect a second QCD phase boundary line, to turn down, steeply, from the continuing deconfinement line, and become the site of hadronization.
- (4) Finally, to the more trivial side, we might expect to turn away from the QCD transition line because the collisional volume does not (or not predominantly) enter the deconfined phase, to begin with. However, recent hadron transport model studies⁶⁷ consistently predict maximum energy densities well above one GeV/fm³ to be reached at this energy, indicating an onset of deconfinement¹⁸ to occur at lower energies.

We conclude that, neither the theoretical foundation, nor the approaches toward an experimental evidence, have been receiving even remotely such an attention recently as we witnessed in the attempts to work out the QCD phase diagram at modest μ_B , where Lattice QCD is applicable.

References

1. F. Karsch and E. Laermann, in Quark-Gluon Plasma 3, ed. H.C. Hwa and X.N. Wang, World Scientific 2004, p.1; Z. Fodor and S.D. Katz, Landolt-Boernstein 23(2010)227, arXiv:0908.3343

2. G. Enrodi, Z.Fodor, S.D.Katz, and K.K.Szabo, JHEP 1104(2011)001; O. Kaczmarek et al., Phys.Rev.D83(2011)014504
3. A. Bazavov et al., arXiv:1509.05786
4. F. Becattini and R.Fries, Landolt-Boernstein 23(2010)208, arXiv:0907.1031; R.Stock, arXiv nucl-th/0703050
5. P. Braun-Munzinger, K.Redlich, and J.Stachel, in Quark-Gluon Plasma 3, eds. H.C.Hwa and X.N.Wang, World Scientific 2004, p.491
6. F. Becattini, M.Gadzicki, A.Keranen, J.Manninen and R.Stock, Phys.Rev. C69(2004)024905
7. A.Andronic, et al., Nucl.Phys. A772(2006)167, and Phys.Lett. B673(2009)142
8. J.Rafelski and M.Danos, Phys. Lett. B97(1980)167;
A.Tounsi and K.Redlich, J.Phys.G28(2002)2095;
W.Florkowski, W.Broniowski and M.Michalec, Acta Phys. Polon. B33(2002)761
9. R.Stock, Phys.Lett. B456(1999)761
10. P.Braun-Munzinger, J.Stachel and C.Wetterich, Phys.Lett.B598(2004)61
11. U.Heinz and G.Kestin, arXiv nucl-th/0612105
12. A.Andronic, P.Braun-Munzinger, K.Redlich and J.Stachel, Nucl.Phys.A904-905(2013)535
13. D.Amati and G.Veneziano, Phys.Lett.B83(1979)87
14. B.R.Webber, Nucl.Phys.B238(1984)492
15. F.Becattini, Nucl.Phys. A702(2002)336
16. N.Cabibbo and G.Parisi, Phys.Lett.B59(1975)67
17. F.Karsch, K.Redlich and A.Tawfik, Phys.Lett. B571(2003)67
18. A.Bozavov et al., Phys.Rev. D90(2014)094503, and Phys.Rev.Lett.113(2014)072001
19. F.Karsch, J.Phys.G38(2011)124098;
S.Mukherjee, Nucl.Phys.A904-905(2013)873
20. C.Ratti et al., Nucl.Phys.904-905(2013)802
21. M.A.Stephanov, J.Phys.G38(2011)124147
22. C.Schmidt et al., Nucl.Phys.A904-905(2013)865;
S.Datta, R.V.Gavai and S.Gupta, ibidem p.883
23. C.Nonaka and M.Asakawa, Phys.Rev.C71(2005)044904;
R.A.Lacey et al., Phys.Rev.Lett.98(2007)092301
24. M.Gazdzicki, M.Gorenstein and P.Seyboth, Acta Phys.Polon. B42(2011)307, arXiv:1006.1765 (hep-ph)
25. L.McLerran and M.Pisarski, Nucl.Phys.A796(2007)83;
A.Andronic et al., Nucl.Phys. A837(2010)65
26. F.Becattini et al., Phys.Rev.C85(2012)044291, arXiv:1201.6349
27. F.Becattini et al., Phys.Rev.Lett.111(2013)082302, arXiv:1212.2431
28. R.Hagedorn, Nuovo Cimento Suppl. 3(1965)147
29. H.Petersen et al., Phys.Rev.C78(2008)044901
30. F.Becattini, J.Steinheimer, R.Stock and M.Bleicher, arXiv:1605.09694
31. R.Snellings, arXiv:1411.7690;
X.Zhu, F.Meng, H.Song and Y.X.Liu, arXiv:1501.0328
32. J.Cleymans, H.Oeschler, K.Redlich and S.Wheaton, Phys.Rev. C73(2006)034905
33. H.T.Ding, Nucl.Phys. A931(2014)52, and references therein
34. S.Bass and A.Dumitru, Phys.Rev.C61(2000)064909;
D.Teaney and E.V.Shuryak, Nucl.Phys.A698(2002)479
35. D.H.Rischke, Y.Pursun and J.A.Maruhn, Nucl.Phys.595(1995)383
36. J.Steinheimer, S.Schramm and H.Stoecker, Phys.Rev.C84(2011)045208
37. J.D.Bjorken, Phys.Rev. D27(1983)140

38. P.Huovinen and H.Petersen, *Eur.Phys.J.A*48(2012)171
39. R.Rapp and E.V.Shuryak, *Phys.Rev.Lett.* 86(2001)2980
40. A.Palmese, W.Cassing, E.Seifert, T.Steinert, P.Moreau and E.Bratkovskaya, *Phys.Rev.C*94(2016)044912
41. M.Floris et al., ALICE Coll., *Nucl.Phys.A*931(2014)103
42. T.Anticic et al., NA49Coll., *Phys.Rev.C*83(2011)014901, and references there
43. A.Ahmad et al., E891 Coll., *Phys.Lett.B*382(1996)35;
L.Ahle et al., E802 Coll., *Phys.Rev.C*60(1999)064901;
S.Albergo et al., E896 Coll., *Phys.Rev.Lett.*88(2002)062301;
J.Barette et al., E887 Coll., *Phys.Rev.C*62(2000)024901
44. L.Kumar, *Nucl.Phys.A*904-905(2013)256
45. P.Alba et al., *Phys.Rev.C*92(2015)064910 and arXiv:1606.06542
46. R.Bellwied et al., arXiv:1305.6297
47. A.Andronic, P.Braun-Munzinger and J.Stachel, *Phys.Lett.B*673(2009)142;
J.Cleymans et al., *Phys.Rev.C*73(2006)034905;
J.Stachel et al., *J.Phys.Conf.Ser.*509(2014)012019;
G.Agakishiev et al.,HADES Coll.,*Eur.Phys.J.A*52(2016)178;
X.Lopez et al.,FOPI Coll.,*Phys.Rev.C*76(2007)052203
48. T.Galatyuk,talk at Erice Nucl.Coll.School 2016
49. U.Heinz, nucl-th/9810056
50. H.Appelshaeuser et al.,NA49Coll.,*Eur.Phys.J.C*2(1998)611
51. A.Wroblewski, *Acta Phys. Pol.*B16(1985)379
52. Ch.Blume et al.,NA49Coll.,nucl-ex/0701042
53. I.G.Baerden et al., BRAHMS Coll., *Phys.Rev.Lett.*90(2003)102301
54. R.Stock,Landolt-Boernstein 1-21A(2008)7.1; nucl-ex/0807.1610
55. J.Adams et al., STAR Coll., *Phys.Rev.Lett.*92(2004)182301;
M.Lamont et al., STAR Coll.,*J.Phys.G*32(2006)105
56. K.Werner,*Phys.Rev.Lett.*98(2007)152301
57. F.Becattini et al.,*Phys.Rev.*90(2014)054907
58. P.Castorina and H.Satz,*J.Mod.Phys.E*23(2014)1450019
59. F.Becattini, P.Castorina, J.Manninen and H.Satz, *Eur.Phys.J.C*56(2008)49
60. F.Becattini and L.Ferroni, *Eur.Phys.J.C*38(2004)225;
F.Becattini and G.Passaleva, *Eur.Phys.J.C*23(2002)551
61. F.Becattini et al., *J.Phys.G*38(2011)025002
62. J.Adams et al.,ALICE Coll.,arXiv:1606.07424
63. S.Mrowczynski, arXiv:1607.02267
64. P.Braun-Munzinger,V.Koch,T.Schaefer and J.Stachel, *Phys.Repts.*62(2016)76
65. J.Steinheimer,V.Vovchenko,J.Aichelin,M.Bleicher and H.Stoecker, arXiv:1608.03737
66. R.Bellwied et al.,arXiv:1507.07510
67. S.Endres,H.van Hees and M.Bleicher, arXiv:1512.06549